Determination of the Correlation between Conductance and Architecture of Disordered β-amyloid Channels

Brian Meckes
Department of Bioengineering
University of California, San Diego
La Jolla, CA 92093
bmeckes@ucsd.edu

Alan Gillman
Department of Bioengineering
University of California, San Diego
La Jolla, Ca 92093
algillma@ucsd.edu

Abstract

It has been hypothesized that the insertion of cation preferential channels into neuronal cell membranes disrupts homeostasis and function leading to Alzheimer's disease. These channels have been shown to be composed of variable numbers of subunits. The nonhomogenous configuration of these subunits in the channels has introduced difficulties in defining set values of ion conductance. Here we model β-amyloid (Aβ) channels as a cylinder spanning the cell membrane of variable radius dependent on subunit configuration. Various subunit motifs were examined and the expected conductance for each configuration determined. The theoretically determined conductance was then compared to experimentally observed values and a new mechanism for pore growth through successive subunit addition is proposed. This work will allow for the introduction of these channels into electrodynamic models of neurons to illuminate the effects of channel insertion into the cell membrane and expand our understanding of neurodegenerative diseases.

1 Introduction

Alzheimer's disease (AD) is a class of protein misfolding disease resulting in neurotoxicity and neurodegeneration. AD is characterized by the formation of fibrils by β-amyloid (Aβ) in the brain, the 1-42 fragment of the Amyloid Precursor Protein. Fibril formation was initially thought to lead to acute cell death, but mounting evidence suggests that these fibrils do not contribute to toxicity[1, 2]. The basic mechanism of physiological pathology is a loss of ionic homeostasis facilitated by oligomers of Aβ, inducing oxidative stress on the cells. Oxidative stress apoptosis results from persistent cellular destabilization by the oligomers[3].

The mechanism of oligomeric Aβ toxicity is poorly understood, with receptor binding, lipid fluidity and thinning, and activation of signaling factors all leading to the accumulation of oxidative reagents, being suggested as possible causes. Recent evidence suggests that Aβ can form channels that are cation preferential[4, 5]. This results in a direct path for loss of ionic homeostasis as ions can enter neurons through these pores. Reconstitution of Aβ monomers into bilayers results in ionic conductance shortly after the bilayer is deposited over a pored[4]. Due to the disordered nature of the proteins resulting in varying oligomer lengths, the conductance observed varies widely, this is thought to be primarily due to the inconsistent diameter size created by having pores composed of varying numbers of monomers and subunits (Figure 1). AFM images of reconstituted Aβ show the presence channel like structures with varied subunit configurations ranging from 3 to 6 subunits[5]. Molecular dynamics simulations also indicate that the oligomers can form stable pore structures of different sizes[6, 7]. However, little is known about the mechanism of channel formation and the dynamics of conformation change.

This work examines how the conductances observed experimentally are related pore structure. This is accomplished through modeling the structure of protein pores with different numbers of oligomer subunits and also varying the number of Aβ monomers in each subunit. Pore diameters and conductances were subsequently calculated for each conformation. The selectivity of the pores also widely varies in electrical recording experiments and can result in non-specific ionic flux. To better understand ion selectivity of the pores, the electric fields for different pore geometries were calculated. This work provides better understanding of how Aβ channels form and the properties associated with them. This will be important for future models of neuronal activity simulating the conditions present in AD and how it impacts cellular dynamics and connectivity.

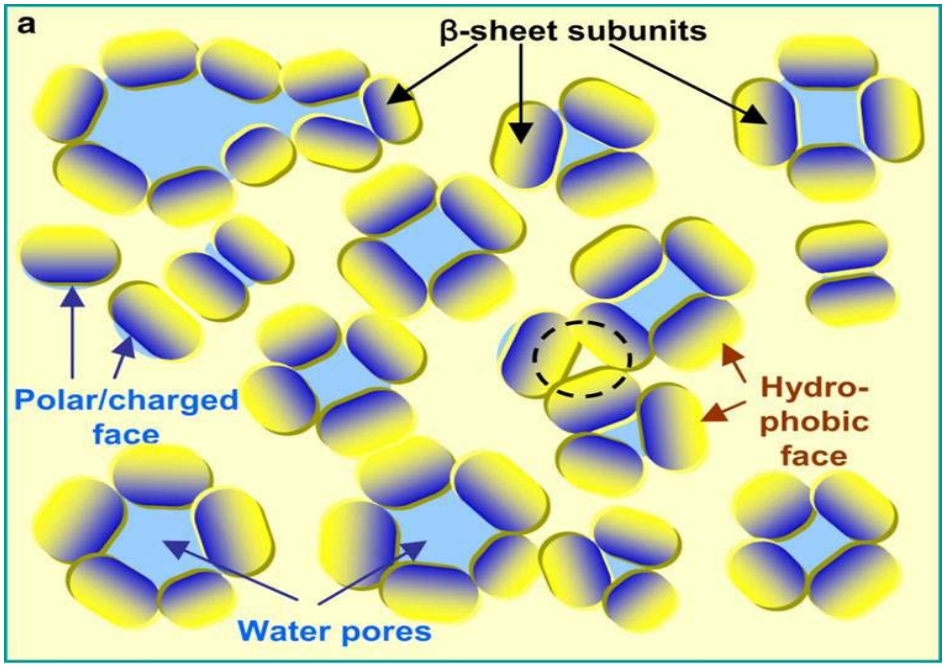

Figure 1: Molecular dynamics (MD) simulations suggest that Aβ channels are dynamic in nature and non-uniform in size and shape. Modified from Jang et al. (2009) [6]

2 Methods

2.1 Model geometry

The complex, dynamic, and undefined geometry of Aβ pores present a challenge for effective modeling. The system was thus modeled under a simplified geometry to allow for comparison between configurations. Each pore subunit was assumed to be a cylinder composed of equal numbers of Aβ monomers. The diameter of each subunit was assumed to be equal to the width of the monomers within and the length equal to that of a cell membrane, 5 nm. Each monomer was assumed to be a cylinder with a diameter of 1 nm based on the findings of Stine et al. [8]. The pore was formed by arranging the subunits such that the subunit centers were positioned at the vertices of a regular polygon. The conducting pore radius could thus be calculated from the difference in the area of the polygon and the bound subunit fraction based on the equation:

$$A_{Pore} = \frac{n^2 N}{4\tan\left(\frac{\pi}{N}\right)} - \left(\frac{N-2}{2}\right)\frac{\pi n^2}{4}$$

$$R_{pore} = \sqrt{\frac{A_{pore}}{\pi}}$$

where N is the number of subunits and n is the number of monomers per subunit.

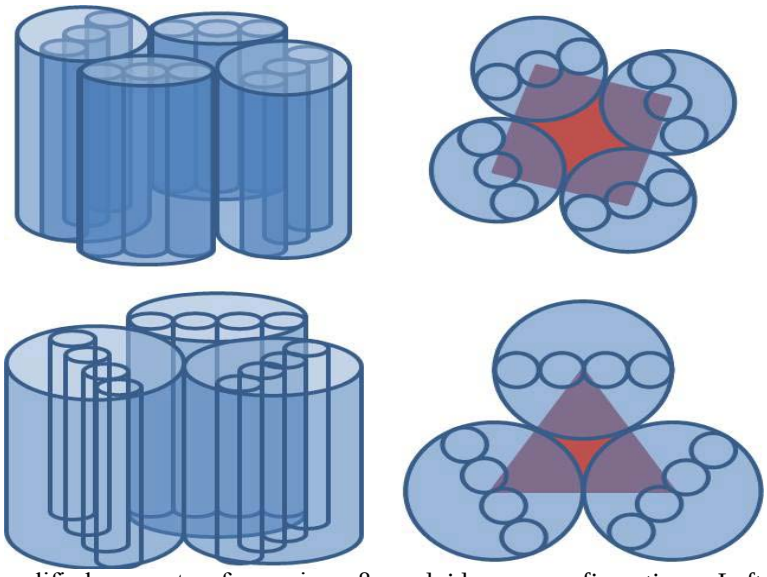

Figure 1: Simplified geometry for various β-amyloid pore configurations. Left: Pores were formed by the aggregation of cylindrical subunits comprised of equal numbers of subunits. Right: The conducting area of the pore (red) is calculated from the difference in area between the polygon and bound subunit fraction (overlap of blue and red).

2.2 Conductance modeling

The equations derived by Tagliazucchi et al. [9] for charged conducting pores was modified to fit the parameters of the Aβ model. Two pore scenarios were modeled: 1) Charge residing solely within the pore, 2) Charge extending onto the surrounding membrane.

Scenario I: Charge residing exclusively within the pore

The resistivity of the pore is calculated by the equation:

$$\Omega = \frac{1}{2R_{pore}\sigma_s} + \frac{1}{\pi}\frac{C_{salt}L}{\rho_g\sigma_s R_{pore}}$$

where C_{salt} is the solution concentration, σ_s the solution resistivity, $\rho_g$the surface charge density, and L the pore length.

Scenario II: Charge extending onto surrounding lipid bilayer

$$\Omega = \frac{1}{\pi\sigma_s}\left[\frac{2C_{salt}}{\rho_g}\left(\ln\left(R_{pore} + \frac{1}{2}\frac{\rho_g}{C_{salt}}\right) - \ln\left(R_{pore}\right)\right)\right] + \frac{1}{\pi}\frac{C_{salt}L}{\rho_g\sigma_s R_{pore}} + \left(\frac{1}{2} - \frac{1}{\pi}\right)\frac{1}{\sigma_s R_{pore}}$$

For both scenarios, the system was modeled in $150\ mM$ KCl solution with a solution resistivity of $1.5\ S/m$ [10]. Based on the primary structure of Aβ, each monomer has a charge of -3 at physiological pH. The surface charge density of the pore is thus calculated as:

$$\rho_g = \frac{3Nn}{2\pi R_{pore} L}$$

The conductance of the pore, calculated as the inverse of resistivity, for each scenario was determined for three to ten subunit pores composed of one to six monomers per subunit.

2.3 Electric field modeling

In addition to modeling the conductance through the pore, the electric field within the pore was modeled. Point charges, corresponding to the overall charge of each subunit, were spatially distributed around the pore at the vertices of the bounding polygon. The resultant electric field at every point within the pore, resulting from the superposition of the contribution from each individual point charge, was calculated via Coulomb's law:

$$E = \sum_{i=1}^{n_Q} \frac{1}{4\pi\epsilon\epsilon_0} \frac{Q_i}{r_i^2} \hat{r}_i$$

3 Results

3.1 Pore Radius

Using the model discussed in section 2.1, varying numbers of subunits and monomers were analyzed and the radius of each geometry was calculated in Matlab (Table 1). Increasing the number of subunits and monomers results in increased pore radius.

Table 1: Radius (nm) of Different Pore Geometries. Cells highlighted in blue correspond with those in Table 2 (to be discussed later)

Radius		Number of Monomers					
		1	2	3	4	5	6
Number of Subunits	3	0.11	0.23	0.34	0.45	0.57	0.68
	4	0.26	0.52	0.78	1.05	1.31	1.57
	5	0.42	0.83	1.25	1.66	2.08	2.49
	6	0.57	1.14	1.72	2.29	2.86	3.43
	7	0.73	1.46	2.19	2.92	3.65	4.38
	8	0.89	1.77	2.66	3.55	4.44	5.32
	9	1.05	2.09	3.14	4.18	5.23	6.27
	10	1.20	2.41	3.61	4.82	6.02	7.22

3.2 Pore Conductances

The conductances calculated for scenario I (Table 2) show that larger pores are more conducting than smaller pores, as expected. The blue highlighted cells in Table 2 demonstrate the difficulty in calculating pore diameter from observed conductances (Figure 4) as multiple subunit conformational motifs (different number of monomers and subunits) result in the same conductance value. From examination of Table 1, this is not strictly driven by radius as the radii of these pores are not the same, indicating that the net charge, which is determined by the total number of monomers, also contributes to the conductance.

Table 2: Conductance (nS) of Aβ pore for Scenario I. Cells highlighted in blue demonstrate the difficulty in correlating an experimentally derived conductance with a pore diameter – different subunit motifs produce identical conductance.

Scenario I		Number of Monomers					
		1	2	3	4	5	6
Number of Subunits	3	0.31	0.61	0.92	1.22	1.53	1.83
	4	0.66	1.31	1.97	2.62	3.28	3.93
	5	1.00	1.99	2.99	3.99	4.99	5.98
	6	1.33	2.67	4.00	5.33	6.66	8.00
	7	1.67	3.33	5.00	6.66	8.33	9.99
	8	2.00	3.99	5.99	7.98	9.98	11.97
	9	2.32	4.65	6.97	9.29	11.62	13.94
	10	2.65	5.30	7.95	10.60	13.25	15.90

Introducing charge on the surrounding membrane, which replicates the effect of having charged lipids, results in the reduction of the conductance dynamic range for Scenario II (Table 3) (0.68-10.36 nS) as compared to Scenario I (Table 2) (0.31-15.90 nS). The charged lipids are negatively charged, which draws cations towards the surface. When the pore is small, this increases the proximity of cations around the pore, effectively drawing cations toward the pore and increasing the likelihood of transport across the membrane. The Tagliazucchi model indicates that there are two important regions that dictate conductance through a charged pore: 1) A hemisphere with the same diameter as the pore directly above the conducting region, 2) The bulk fluid and surface surrounding the pore. When the surface is uncharged, the hemisphere dominates the conductance – for a large pore there is a large electric field within the hemisphere, which draws cations toward the pore. However, when the membrane is charged, the radius of the charged hemisphere increases and draws cations toward a region larger than the pore itself. Whereas the cations in the uncharged scenario were funneled toward a region of the same size as the pore, the charged membrane brings ions to a region with a larger footprint than the pore. This effectively shields the pore by diminishing the probability of cation interaction with the pore, as compared to the uncharged membrane scenario. In other words, cations get trapped on the lipid membrane near the pore surface, reducing the ionic flux. Since transport is a probabilistic event, a charged membrane increases the chances of ionic transport in small pores while decreasing the probability in a large pore. Since ionic transport is equivalent to conductance, small pores will see greater conductance while large pores will have lower conductance for Scenario II (Table 3) as compared to Scenario I (Table 2).

Table 3: Conductance (nS) of Aβ pores for Scenario II.

Scenario II		Number of Monomers					
		1	2	3	4	5	6
Number of Subunits	3	0.68	1.32	1.91	2.46	2.98	3.46
	4	1.30	2.43	3.42	4.29	5.06	5.75
	5	1.83	3.33	4.57	5.62	6.50	7.25
	6	2.30	4.10	5.51	6.65	7.56	8.30
	7	2.75	4.77	6.30	7.47	8.37	9.07
	8	3.16	5.38	6.97	8.13	8.99	9.63
	9	3.55	5.91	7.54	8.68	9.48	10.05
	10	3.91	6.40	8.03	9.12	9.86	10.36

3.2 Electric Field in Pores

The effect of electric field on the cation selectivity of Aβ pores was examined. Figure 3 shows the electric field in two different pores, one with a small pore radius (left) and the other with a large pore radius (right). The octomer (right) exhibits more diffuse low field strength regions than the trimer (right). Additionally, the low field regions in the octomer extend further from the pore center than in the trimer. This suggests that that electrostatics play less of a role in ion conductance through large pores than small pores and large pores are thus less cation selective.

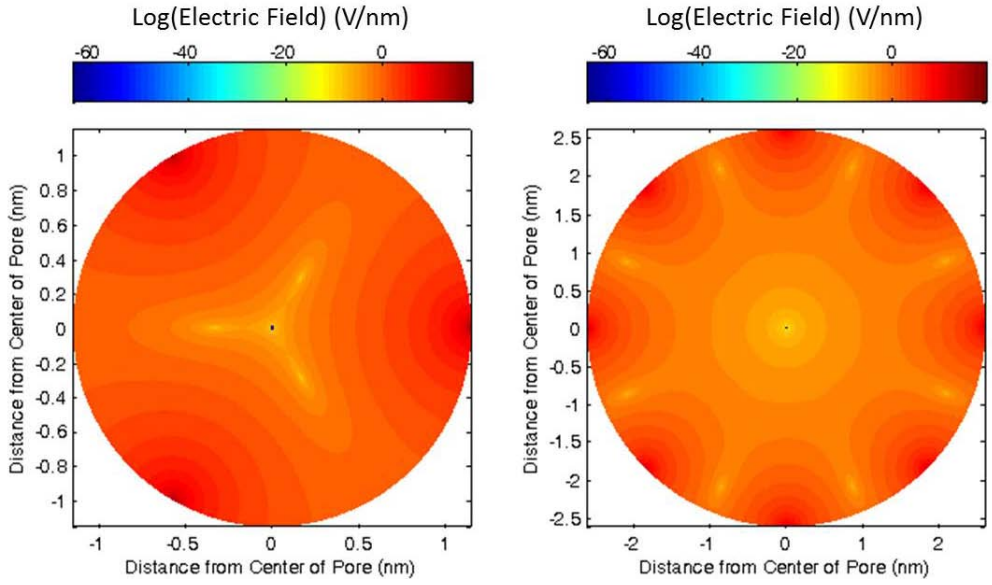

Figure 3: Aβ Pores become less cation selective as the diameter increases. The resultant electric field within pores is shown as a heat map with areas of high field strength appearing in red and low field strength appearing yellow. The plot on the left is for a trimer of dimers (three

subunits with two monomers per subunit) while the right shows an octomer of dimers (eight subunits with two monomers each).

4 Conclusion

Comparing experimental (Figure 4) data to the theoretical results presented here indicates that most pores are of a small diameter. This agrees with current understanding of Aβ pore formation that suggests that smaller pores are more stable than large pores, as increasing the pore radius would result in a structure that collapses. This is supported by the experimental results indicating that most conductance are less than 0.7 nS, which correlates to pores of 3-4 subunits based on theoretical estimates of pore conductances (Table 1 and 2).

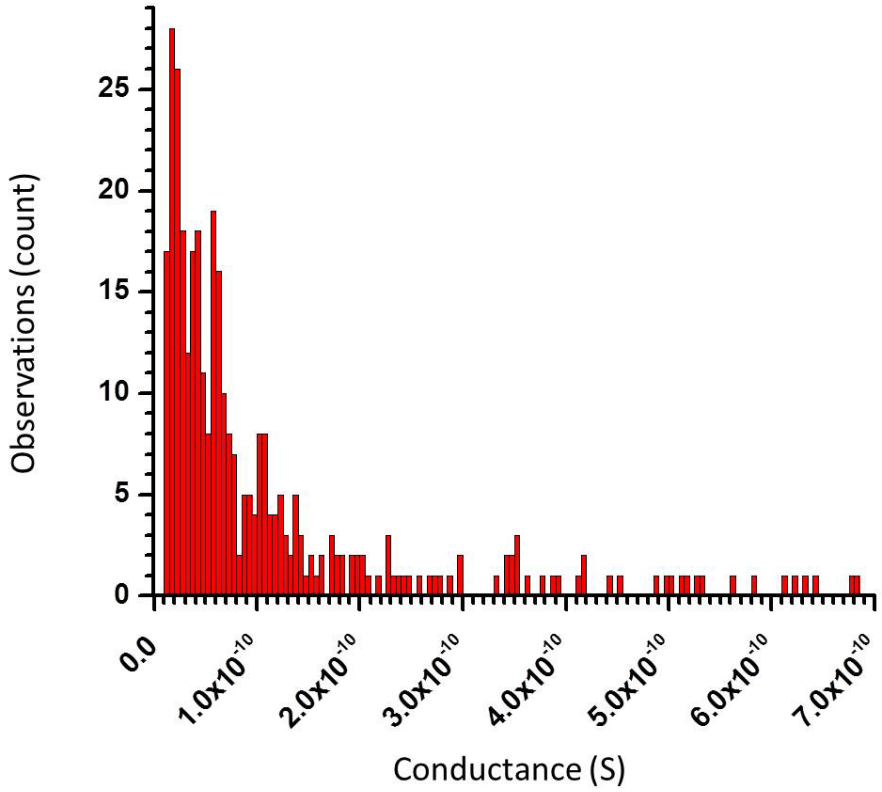

Figure 4: Experimentally observed conductance of Aβ pores. Electrical recording of lipid bilayers was carried out with Aβ added to the media. The integrity of the membrane was ensured via lack of conductance prior to protein addition. Step changes in the conductance were recorded. The histogram shows that extremely low conductance (pS scale) steps dominate the recording. This suggests growth of small pores (3-4 subunits) through successive subunit addition rather than spontaneous assembly of large pores with high (nS scale) conductance.

The data contained in Figure 4 also shows conductances that occur as a result of conformational change (i.e. the conductance is measured at one value and then a step increase occurs resulting in a higher conductance value and the change in conductance is reported). This suggests that the pore has increased in diameter by a small amount resulting in slight increase in conductance, as the change in conductance observed is less than any of the conductances predicted by the models. This change in conductance indicates that a new pore has not formed in the bilayer, but a small pore has become larger. Large pores are unlikely to form via spontaneous aggregation of subunits within the cellular membrane, but rather through successive growth of small pores through subunit addition (Figure 5), which is supported by our analysis. The larger pore will exhibit a small step increase in conductance as the size grows.

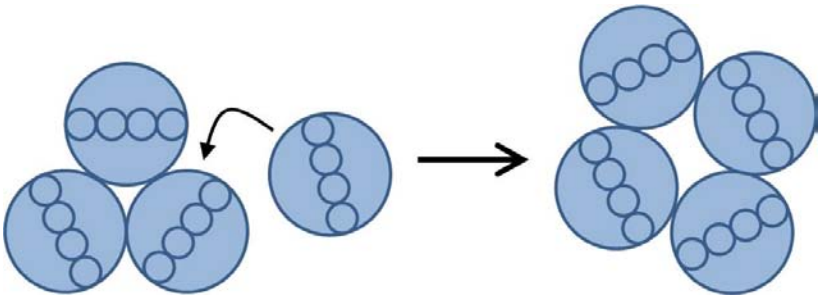

Figure 5: Proposed model for successive subunit addition and pore expansion. A pore of 3 subunits is expanded to a pore consisting of 4 subunits via subunit addition.

Future work in this area will focus on testing new geometric configurations to resolve differences between the values obtained via the model and experimental data. The current model, while geometrically convenient does not necessarily represent the proper configuration of Aβ pores in biology. The true structure of the subunits is likely more elongated and elliptical than the idealized cylinders used for the present analysis. Future simulations will focus on elliptical geometries and varying numbers of monomers within each subunit in the simulation – in this manner, native configurations can be more closely simulated. Additionally, the effects of the modeled Aβ conductance on spiking neurons will be modeled to simulate the pathophysiology of amyloid diseases such as Alzheimer's. Furthermore, the effects of Aβ pore toxicity, whether in a single cell or in multiple cells in small networks of cells, will be examined to help determine how cell impairment affects single cell dynamics and neural connectivity.

Acknowledgments

The authors acknowledge and thank Dr. Ricardo Capone for helpful discussions and access to experimental data

References

1. Bhatia, R., H.A.I. Lin, and R. Lal, *Fresh and globular amyloid ÃŸ protein (1â€“42) induces rapid cellular degeneration: evidence for AÃŸP channel-mediated cellular toxicity.* The FASEB Journal, 2000. **14**(9): p. 1233-1243.

2. Bucciantini, M., et al., *Inherent toxicity of aggregates implies a common mechanism for protein misfolding diseases.* Nature, 2002. **416**(6880): p. 507-511.

3. Mattson, M.P. and S.L. Chan, *Calcium orchestrates apoptosis.* Nature cell biology, 2003. **5**(12): p. 1041-1043.

4. Capone, R., et al., *Amyloid-beta-induced ion flux in artificial lipid bilayers and neuronal cells: resolving a controversy.* Neurotoxicity research, 2009. **16**(1): p. 1-13.

5. Quist, A., et al., *Amyloid ion channels: A common structural link for protein-misfolding disease.* Proceedings of the National Academy of Sciences of the United States of America, 2005. **102**(30): p. 10427-10432.

6. Jang, H., et al., *Misfolded Amyloid Ion Channels Present Mobile β-Sheet Subunits in Contrast to Conventional Ion Channels.* Biophysical journal, 2009. **97**(11): p. 3029-3037.

7. Jang, H., et al., *New structures help the modeling of toxic amyloidß ion channels.* Trends in Biochemical Sciences, 2008. **33**(2): p. 91-100.

8. Stine Jr, W.B., et al., *In vitro characterization of conditions for amyloid-β peptide oligomerization and fibrillogenesis*. Journal of Biological Chemistry, 2003. **278**(13): p. 11612-11622.

9. Tagliazucchi, M., Y. Rabin, and I. Szleifer, *Ion Transport and Molecular Organization Are Coupled in Polyelectrolyte-Modified Nanopores*. Journal of the American Chemical Society, 2011. **133**(44): p. 17753-17763.

10. Wu, Y.C. and W.F. Koch, *Absolute determination of electrolytic conductivity for primary standard KCl solutions from 0 to 50 C*. Journal of solution chemistry, 1991. **20**(4): p. 391-401.